

# Hadronic Spectra from Deformed AdS Backgrounds

Eduardo Folco Capossoli<sup>1,2,\*</sup>, Miguel Angel Martín Contreras<sup>3,†</sup>

Danning Li<sup>4,‡</sup>, Alfredo Vega<sup>3,§</sup> and Henrique Boschi-Filho<sup>1¶</sup>

<sup>1</sup>*Instituto de Física, Universidade Federal do Rio de Janeiro,  
21.941-972 - Rio de Janeiro-RJ - Brazil*

<sup>2</sup>*Departamento de Física / Mestrado Profissional  
em Práticas da Educação Básica (MPPEB),*

*Colégio Pedro II, 20.921-903 - Rio de Janeiro-RJ - Brazil*

<sup>3</sup>*Instituto de Física y Astronomía, Universidad de Valparaíso,  
A. Gran Bretaña 1111, Valparaíso, Chile*

<sup>4</sup>*Department of Physics and Siyuan Laboratory,  
Jinan University, Guangzhou 510632, China*

## Abstract

Because of the presence of modified warp factors in metric tensors, we use deformed AdS<sub>5</sub> spaces to apply the AdS/CFT correspondence to calculate the spectra for even and odd glueballs, scalar and vector mesons, and baryons with different spins. For the glueball cases, we derive their Regge trajectories and compare them with those related to the pomeron and the odderon. For the scalar and vector mesons as well as baryons the determined masses are compatible with the PDG. In particular for these hadrons we found Regge trajectories compatible with another holographic approach as well as with the hadronic spectroscopy, which present an universal Regge slope of approximately 1.1 GeV<sup>2</sup>.

Keywords: hadronic spectra, AdS/QCD model, Regge trajectories

---

\* eduardo\_capossoli@cp2.g12.br

† miguelangel.martin@uv.cl

‡ lidanning@jnu.edu.cn

§ alfredo.vega@uv.cl

¶ boschi@if.ufrj.br

## I. INTRODUCTION

Quantum Chromodynamics (QCD) is a non-Abelian quantum field theory employed for dealing with strong interactions. Although it boasts enormous success in the high energy regime, the use of QCD is difficult when investigating processes that occur at low energies (IR regions) because of the failure of the perturbative approach. This peculiar feature of the QCD is related to the fact that it is a confining theory in the IR, implying that only bound states of quarks or gluons are observed.

Hadronic spectroscopy is a highly interesting field with regard to the application of new approaches to extract information about hadronic properties, given that results are comparable with the experimental data.

Among several techniques to handle within the field of Hadronic spectroscopy, there is one that emerged in 1997 proposed by Juan Maldacena, referred to as the Anti de Sitter/Conformal Field Theory or AdS/CFT correspondence [1–5]. This correspondence is very useful, as it provides guidance on how to relate a weak coupling theory, which is in this case represented by a superstring theory in a ten-dimensional curved space, named  $AdS_5 \times S^5$  with a strong coupling theory which is a super conformal Yang-Mills theory with extended supersymmetry  $\mathcal{N} = 4$ , symmetry group  $SU(N \rightarrow \infty)$  in a flat four-dimensional Minkowski space.

However, the AdS/CFT correspondence cannot be used directly to reproduce QCD, as the latter is not a conformal theory, as it possesses numerous different scales (masses, critical temperature, etc.). v Some proposals appeared to break the conformal invariance and build effective theories known as AdS/QCD models, e.g, the hardwall model. In this model, the conformal symmetry is broken via introduction of a hard IR cutoff at a certain value  $z_{max}$  of the holographic coordinate  $z$  and by considering only a slice of the  $AdS_5$  space within the interval  $[0, z_{max}]$  [6–8]. Achievements in hadronic spectroscopy within the hardwall are presented in several studies [9–15].

Another example of breaking the conformal invariance is given by the softwall model. In this model a soft IR cutoff via an introduction of a dilaton field in the action. This approach was proposed in [16] to study mesonic spectroscopy. Usually, this model is referred to as the original softwall model. Several modifications of this model were considered subsequently to deal with hadronic spectroscopy as presented in e.g., Refs. [17–26]. Further addressing

some modification in the Refs.[27–32], instead of the introduction of a dilation in the action, a modified warp factor in the AdS metric was considered. Particularly, in Ref. [29] such a modification was proposed to study hadronic spectroscopy. Other modifications of the softwall model were used in Refs. [28, 30, 31] to discuss the quark-antiquark potential and in Ref. [32] to deal with scalar and tensor glueballs. One open problem associated with the softwall model is the sign of the dilaton. In the original case, the dilaton is an exponential with a negative argument [16]. In Refs. [33–35], authors argued that a positive dilaton is preferred, which the authors of Ref. [36] disagree with. These authors also point out that a positive dilaton implies the existence of a massless scalar in the spectrum.

In this study, inspired by Refs. [27–29], we investigate these problems with modified warp factors in the  $AdS_5$  metric instead of introducing dilaton fields in the action. In this sense, in our set-up we consider deformed AdS backgrounds. Subsequently, using this approach, we compute the hadronic spectra for several particles with different spins. We employ the same form for the warp factor in the metric by fitting the free parameter in each case. The values of the parameters are observed to be different for each sector. This scenario is similar to the case of the original softwall model, where different dilaton fields are needed for each particle sector. The main advantage of our approach is that we can also directly deal with fermions, contrary to the original softwall model. Furthermore, our approach provides appropriate masses and Regge trajectories, for instance, for odd and even spin glueballs.

This paper is organized as follows. In Section II we present a brief review of the original softwall model and our deformed AdS background. In Section III, we apply our model to the even and odd spin glueball states. In Section IV, we study the case of scalar mesons obtaining their spectra. We calculate the hadronic spectra for the vector mesons in Section V and in Section VI we address the baryonic case with spins  $1/2$ ,  $3/2$  and  $5/2$ . For those particles, we also obtain the corresponding Regge trajectories. In particular, for the glueballs we derive the Regge trajectories related to the pomeron and the odderon. Finally, in Section VII we present the conclusions and final comments.

## II. SOFTWALL MODEL AND DEFORMED ADS SET-UP

There are at least two interesting reasons behind the emergence of the softwall model. The first is related to the introduction of the soft IR cutoff instead a hard cutoff as in the

hardwall model, as this approach seems more natural. The second reason lies in the fact that the softwall model truly yields linear Regge trajectories, which was an established behavior since the beginning of hadronic spectroscopy, so that

$$J(m) \approx \alpha' m^2 + \alpha_0, \quad (1)$$

where  $J$  is the total angular momentum;  $m$  represents the hadronic mass;  $\alpha'$  (Regge slope) and  $\alpha_0$  are constants. The relationship between radial excitation  $n$  and its squared hadron mass, given by:

$$m^2 \approx \beta' n + \beta_0, \quad (2)$$

with  $\beta'$  and  $\beta_0$  as constants.

In the original formulation of the softwall model, the action of the fields, up to some constant, is described by:

$$S = \int d^5x \sqrt{-g} e^{-\Phi(z)} \mathcal{L}, \quad (3)$$

where  $\Phi(z)$  is the dilaton field, usually given by  $\Phi(z) = kz^2$ , where  $|k| \sim \Lambda_{QCD}^2$ , and  $\mathcal{L}$  is the Lagrangian density.

The main difference between the original softwall model and the present study is the modified  $AdS_5$  metric tensor using an exponential warp factor for all glueballs and hadrons. In Ref. [29] the authors used different warp factor profiles, usually logarithmic ones, for each hadronic sector.

As we employ the same warp factor profile in the AdS space for all glueballs and hadrons, we refer the approach of this study as a deformed  $AdS_5$  background. Then, we write the deformed  $AdS_5$  metric as:

$$ds^2 = g_{mn} dx^m dx^n = \frac{R^2}{z^2} e^{kz^2} (dz^2 + \eta_{\mu\nu} dx^\mu dx^\nu) = e^{2A(z)} (dz^2 + \eta_{\mu\nu} dx^\mu dx^\nu), \quad (4)$$

where  $R$  is the usual AdS radius (from here onward, we assume  $R = 1$  throughout this text),  $\eta_{\mu\nu}$  is the flat Minkowski space metric tensor in four dimensions with signature  $(-, +, +, +)$ ,  $z$  is the holographic coordinate, and  $x^m = (z, x^\mu)$  for  $\mu = 0, \dots, 3$ . The warp factor  $A(z)$  in Eq. (4) can be read as:

$$A(z) = -\log(z) + \frac{kz^2}{2}. \quad (5)$$

In our model, the action for the fields is given as:

$$S = \int d^5x \sqrt{-g} \mathcal{L}, \quad (6)$$

where  $g$  is the determinant of the five-dimensional metric tensor presented in Eq. (4).

### III. HADRONIC SPECTRA FOR GLUEBALLS STATES

Fritzsche and Gell-Mann pointed out in Refs [37, 38]. “If the quark-gluon field theory indeed yields a correct description of strong interactions, there must exist glue states in the hadron spectrum”. This sentence does really reveals the importance of those “glue states” nowadays referred to as glueballs. Glueballs are colorless bound states of gluons predicted by QCD but not experimentally detected to date.

Glueballs are characterized by  $J^{PC}$  where  $J$  (even or odd) is the total angular momentum,  $P$  is the  $P$ -parity (spatial inversion) and  $C$  is the  $C$ -parity (charge conjugation) eigenvalues. For the glueballs case,  $P = (-1)^L$  and  $C = (-1)^{L+S}$ .

Numerous experimental efforts were conducted in the search for glueballs [39–42]. Some theoretical and non-holographic approaches are described in Refs. [43–48]. The holographic approach is presented in Refs. [49–58].

In this study based on a deformed AdS space, we compute the masses of even spin glueballs with  $P = C = +1$  and odd spin glueballs with  $P = C = -1$ . Even spin glueballs with  $P = C = +1$  are particularly interesting, as in the Chew-Frautschi plane, their states lie on the Pomeron Regge trajectory. In contrast, odd spin glueballs with  $P = C = -1$  lie on the odderon Regge trajectory.

We start our calculation using the standard action for a massive scalar field  $X$  in  $5D$  space, given by:

$$S = \int d^5x \sqrt{-g} [g^{mn} \partial_m X \partial_n X + M_5^2 X^2]. \quad (7)$$

From the action (7) one can find the following equations of motion, so that:

$$\partial_m [\sqrt{-g} g^{mn} \partial_n X] - \sqrt{-g} M_5^2 X = 0, \quad (8)$$

where  $g^{mn} = e^{-2A(z)} \eta^{mn}$ .

The Eq. (8) can be written as:

$$\partial_m [e^{3A(z)} \eta^{mn} \partial_n X] - e^{5A(z)} M_5^2 X = 0, \quad (9)$$

with the warp factor  $A(z)$  given in Eq. (5).

Defining  $B(z) = -3A(z)$ , we obtain:

$$\partial_m [e^{-B(z)} \eta^{mn} \partial_n X] - e^{\frac{-5B(z)}{3}} M_5^2 X = 0. \quad (10)$$

Next, we use a plane wave ansatz with the amplitude only depending on the  $z$  coordinate and propagating in the transverse coordinates  $x^\mu$  with momentum  $q_\mu$ ,

$$X(z, x^\mu) = v(z)e^{iq_\mu x^\mu}. \quad (11)$$

After some algebraic manipulation and defining  $v(z) = \psi(z)e^{\frac{B(z)}{2}}$  we obtain a ‘‘Schrödinger-like’’ equation:

$$-\psi''(z) + \left[ \frac{B'^2(z)}{4} - \frac{B''(z)}{2} + e^{\frac{-2B(z)}{3}} M_5^2 \right] \psi(z) = -q^2 \psi(z), \quad (12)$$

with  $B(z) = -3A(z)$  and  $E = -q^2$  as eigenenergies.

### A. Results for even and odd spin glueball spectra

To compute the glueball masses, Eq. (12) must be solved numerically. To this end, from the AdS/CFT dictionary we first relate the masses of supergravity fields in the AdS space ( $M_5$ ) with the scaling dimensions of an operator in the boundary theory ( $\Delta$ ), such that:

$$M_5^2 = (\Delta - p)(\Delta + p - 4), \quad (13)$$

where  $p$  is the index of a  $p$ -form. For the case of the scalar glueball  $0^{++}$  we obtain  $p = 0$ . Because the scalar glueball is dual to the fields with  $M_5 = 0$ , its conformal dimension is  $\Delta = 4$ .

Second, the scalar glueball state is represented on the boundary theory by the operator  $\mathcal{O}_4$ , given by:

$$\mathcal{O}_4 = \text{Tr} (F^2) = \text{Tr} (F^{\mu\nu} F_{\mu\nu}). \quad (14)$$

To raise the total angular momentum  $J$ , we follow Ref. [11] by inserting symmetrised covariant derivatives in a given operator with spin  $S$ , such that the total angular momentum after the insertion becomes  $S + J$ . In the particular case of the operator  $\mathcal{O}_4 = \text{Tr} F^2$ , we obtain:

$$\mathcal{O}_{4+J} = \text{Tr} (F D_{\{\mu_1 \dots \mu_J\}} F), \quad (15)$$

with the conformal dimension  $\Delta = 4 + J$ . For  $J = 0$  we recover  $\Delta = 4$ .

Thus, for even spin glueball states after the insertion of symmetrized covariant derivatives, we obtain:

$$M_5^2 = J(J + 4); \quad (\text{even } J). \quad (16)$$

	Even glueball states $J^{PC}$					
	$0^{++}$	$2^{++}$	$4^{++}$	$6^{++}$	$8^{++}$	$10^{++}$
Masses	0.76	2.08	3.17	4.22	5.26	6.30

Table I. Even glueball masses expressed in GeV from Eq. (17) with warp factor constant  $k$  as  $k_{\text{gbe}} = 0.31^2 \text{ GeV}^2$ .

Hence, we write Eq.(12) as:

$$-\psi''(z) + \left[ \frac{B'^2(z)}{4} - \frac{B''(z)}{2} + e^{\frac{-2B(z)}{3}} J(J+4) \right] \psi(z) = -q^2 \psi(z). \quad (17)$$

Solving Eq.(17), for even glueball states, one obtains the four-dimensional masses presented in Table I.

Using the data from Table I, we plotted a Chew-Frautschi plane, here represented as  $m^2 \times J$ , where  $J$  is total angular momentum, and  $m^2$  is the squared even glueball mass represented by the dots in figure 1. Using a standard linear regression method, we obtain the equation

$$J(m^2) \approx (0.25 \pm 0.02)m^2 + (0.88 \pm 0.51), \quad (18)$$

which represents an approximate linear Regge trajectory associated with the pomeron in agreement with Refs. [59, 60].

In contrast, for odd glueball states, the operator  $\mathcal{O}_6$  that describes the glueball state  $1^{--}$  is given by [14, 51, 61, 62]:

$$\mathcal{O}_6 = \text{Sym Tr} \left( \tilde{F}_{\mu\nu} F^2 \right), \quad (19)$$

where this dual operator creates odd glueball states at the boundary. This operator has the conformal dimension  $\Delta = 6$ , and after the insertion of symmetrized covariant derivatives, we obtain:

$$\mathcal{O}_{6+J} = \text{Sym Tr} \left( \tilde{F}_{\mu\nu} F D_{\{\mu_1 \dots \mu_J\}} F \right), \quad (20)$$

with  $\Delta = 6 + J$ . Therefore,

$$M_5^2 = (J+6)(J+2); \quad (\text{odd } J), \quad (21)$$

and we can rewrite Eq.(12) as:

$$-\psi''(z) + \left[ \frac{B'^2(z)}{4} - \frac{B''(z)}{2} + e^{\frac{-2B(z)}{3}} (J+6)(J+2) \right] \psi(z) = -q^2 \psi(z). \quad (22)$$

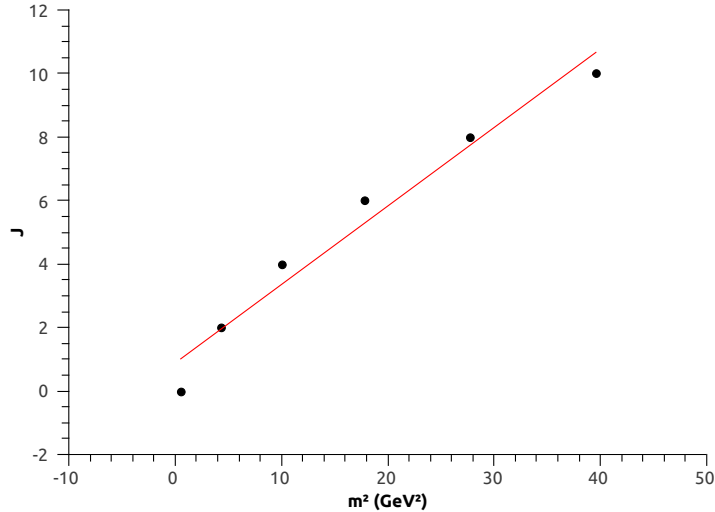


Figure 1. (color online) Approximate linear Regge trajectory associated with the pomeron from Eq. (18). The dots correspond to the masses found in Table I for even glueball states within the deformed  $AdS_5$  space approach .

	Odd glueball states $J^{PC}$					
	1 <sup>---</sup>	3 <sup>---</sup>	5 <sup>---</sup>	7 <sup>---</sup>	9 <sup>---</sup>	11 <sup>---</sup>
Masses	2.63	3.70	4.74	5.78	6.81	7.84

Table II. Odd spin glueball masses expressed in GeV as from Eq.(22) with the warp factor constant  $k$  as  $k_{\text{gbo}} = 0.31^2 \text{ GeV}^2$ .

Solving Eq.(22) for odd glueball states, we obtain the four-dimensional masses presented in Table II.

Using the data in Table II, we plotted a Chew-Frautschi plane  $m^2 \times J$  in figure 2 for odd spin glueballs. Using a standard linear regression method, we obtain the equation

$$J(m^2) \approx (0.18 \pm 0.01)m^2 + (0.47 \pm 0.45), \quad (23)$$

which is in agreement with Ref. [63], within the nonrelativistic constituent model.

Notably, the value for the constant  $k$  in the warp factor  $A(z)$  for even spin glueball represented by  $k_{\text{gbe}}$  and for odd spin glueball represented by  $k_{\text{gbo}}$  have the same numerical value  $k_{\text{gbe}} = k_{\text{gbo}} = 0.31^2 \text{ GeV}^2$ .

To facilitate the comparison between our results with the deformed AdS model and other



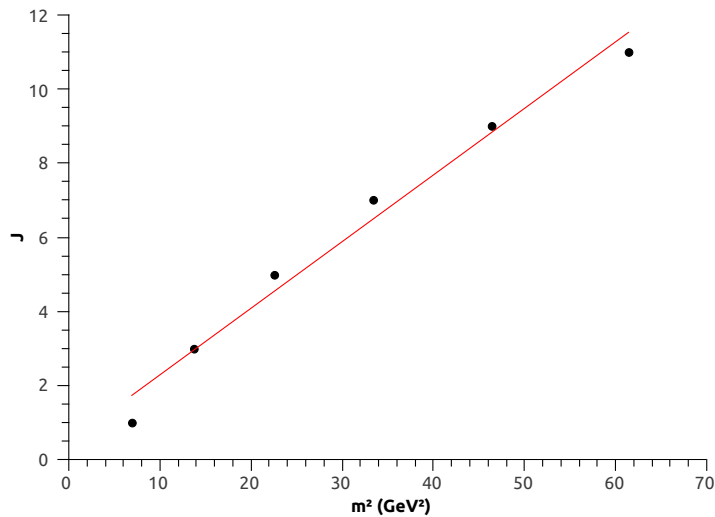


Figure 2. (color online) Approximate linear Regge trajectory associated with the odderon from Eq. (23). The dots correspond to the masses found in Table II within the deformed  $AdS_5$  space approach for odd spin glueballs.

approaches, we summarize several results provided by the literature in Tables III and IV.

Models used	Even Glueball States $J^{PC}$			
	$0^{++}$	$2^{++}$	$4^{++}$	$6^{++}$
$N_c = 3$ lattice [64]	1.475(30)(65)	2.150(30)(100)	3.640(90)(160)	4.360(260)(200)
$N_c = 3$ anisotropic lattice [43]	1.730(50)(80)	2.400(25)(120)		
$N_c = 3$ anisotropic lattice [45]	1.710(50)(80)	2.390(30)(120)		
$N_c = 3$ lattice [46]	1.58(11)			
$N_C \rightarrow \infty$ lattice [46]	1.48(07)			
Constituent models [47]		2.42	2.59	
Constituent models [48]		3.99	3.77	4.60

Table III. Glueball masses for  $J^{PC}$  states expressed in GeV, with even  $J$ , achieved with non-holographic models from the literature. Numbers in parentheses represent uncertainties.

Models used	Odd glueball states $J^{PC}$			
	$1^{--}$	$3^{--}$	$5^{--}$	$7^{--}$
Relativistic many body [63]	3.95	4.15	5.05	5.90
Non-Relativistic constituent [63]	3.49	3.92	5.15	6.14
Wilson loop [65]	3.49	4.03		
Vacuum correlator [66]	3.02	3.49	4.18	4.96
Vacuum correlator [66]	3.32	3.83	4.59	5.25
Semi-relativistic potential [67]	3.99	4.16	5.26	
Anisotropic lattice [45]	3.83	4.20		
Isotropic lattice [44, 64]	3.24	4.33		

Table IV. Glueball masses for  $J^{PC}$  states expressed in GeV, with odd  $J$ , achieved with non-holographic models from the literature.

#### IV. HADRONIC SPECTRA FOR SCALAR MESONS

Mesons are bound states between a quark and an antiquark that can be represented by a spin singlet with total spin  $S = 0$  or a spin triplet with total spin  $S = 1$ . The coupling between  $S$  and the orbital angular momentum  $L$  must be considered, producing a total angular momentum  $J = L$  in the case of the singlet state, and  $J = L - 1, L, L + 1$  in the case of the triplet state.

In mesonic spectroscopy [68], mesons are characterized by  $I^G(J^{PC})$ , where  $I$  is the isospin,  $G$  is the  $G$ -parity defined  $G = (-1)^I = \pm 1$ , and  $P$  is the  $P$ -parity defined for mesons as  $P = (-1)^{L+1}$ . Finally,  $C$  is the  $C$ -parity defined as  $C = (-1)^{L+S}$ . In the boundary theory scalar mesons are represented by the operator:

$$\mathcal{O}_{SM} = \bar{q} D_{\{J_1 \dots J_m\}} q \quad \text{with} \quad \sum_{i=1}^m J_i = J, \quad (24)$$

where  $J$  is the total angular momentum.

In this section we address light scalar mesons, i.e.,  $J = 0$  and unflavored ( $S = C = B = 0$ ).

Within the holographic approach, the description of the scalar glueball ( $gg$ ) and the scalar meson ( $q\bar{q}$ ) is the same; however, the main difference is provided by the bulk mass, which defines the hadron identity. To study the scalar meson, we must start from the action for a massive scalar field (7), which will lead us to the ‘‘Schrödinger-like’’ equation (12).

## A. Results for scalar mesons spectra

Employing the relationship  $M_5^2 = (\Delta - p)(\Delta + p - 4)$ , and identifying  $M_5$  as the scalar meson bulk mass, the index of the  $p$ -form with the total angular momentum ( $p = J = 0$ ) for the scalar meson and  $\Delta$  depicts the conformal dimension, which is  $\Delta = 3$ , as each quark contributes with  $3/2$ . Finally, we rewrite Eq.(12) with  $M_5^2 = -3$  as:

$$-\psi''(z) + \left[ \frac{B'^2(z)}{4} - \frac{B''(z)}{2} - 3 e^{\frac{-2B(z)}{3}} \right] \psi(z) = -q^2 \psi(z), \quad (25)$$

where  $B(z) = -3A(z)$ . Solving (25) numerically with the warp factor constant  $k$  identified as  $k_{\text{sm}} = -0.332^2 \text{ GeV}^2$ , we obtain the masses compatible with the family of the scalar meson  $f_0$ , with  $I^G J^{PC} = 0^+(0^{++})$ , as indicated in table V. The error presented in last column of Table V ( $\%M$ ) is the error defined by:

$$\%M = \sqrt{\left(\frac{\delta O_i}{O_i}\right)^2} \times 100, \quad (26)$$

where  $\delta O_i$  depicts the deviations between the data ( $M_{\text{exp}}$ ) and the model prediction ( $M_{\text{th}}$ ). Throughout the text, in the cases where the experimental is provided at intervals, as the  $f_0(1370)$  state, we use the average value of the interval to evaluate the deviations. We moreover compute the total r.m.s error defined by:

$$\delta_{rms} = \sqrt{\frac{1}{N - N_p} \sum_{i=1}^N \left(\frac{\delta O_i}{O_i}\right)^2} \times 100, \quad (27)$$

where  $N$  and  $N_p$  are the number of measurements and parameters, respectively. From Eq. (27) we find that  $\delta_{rms} = 3.77\%$  for table V.

Using the data from Table V, we plotted a Chew-Frautschi plane represented as  $n \times m^2$ , where  $n$  is the holographic radial excitation and,  $m^2$  is the squared scalar meson mass represented by the dots (our model) or squares (PDG) in figure 3. Using a standard linear regression method we obtain the experimental and theoretical Regge trajectories for the scalar meson  $f_0$  family, such that:

$$m_{Exp}^2 = (0.639 \pm 0.027) n + (0.458 \pm 0.135), \quad (28)$$

$$m_{th}^2 = (0.647 \pm 0.002) n + (0.513 \pm 0.011). \quad (29)$$

The authors of Refs. [70, 71] within a holographic softwall model likewise computed the masses for the  $f_0$  meson family and derived its Regge trajectory slightly differently from Eq.

	Scalar meson $f_0$ ( $0^+(0^{++})$ )			
	$f_0$ meson	$M_{\text{exp}}$ GeV [69]	$M_{\text{th}}$ GeV	$\%M$
$n = 1$	$f_0(980)$	$0.990 \pm 0.02$	1.089	9.97
$n = 2$	$f_0(1370)$	1.2 to 1.5	1.343	0.54
$n = 3$	$f_0(1500)$	$1.504 \pm 0.006$	1.562	3.87
$n = 4$	$f_0(1710)$	$1.723^{+0.006}_{-0.005}$	1.757	1.96
$n = 5$	$f_0(2020)$	$1.992 \pm 0.016$	1.933	2.96
$n = 6$	$f_0(2100)$	$2.101 \pm 0.007$	2.095	0.27
$n = 7$	$f_0(2200)$	$2.189 \pm 0.013$	2.246	2.61
$n = 8$	$f_0(2330)$	$2.337 \pm 0.014$	2.388	2.17

Table V. Masses of light unflavored scalar meson  $f_0$  ( $S = C = B = 0$ ). Column  $n = 1, 2, 3, \dots$  represents holographic radial excitation of scalar mesons. The ground state is represented by  $n = 1$ . Column  $M_{\text{exp}}$  represents the experimental data from PDG [69]. Column  $M_{\text{th}}$  represents masses obtained within the deformed  $AdS_5$  space approach using Eq.(25) with  $k_{\text{sm}} = -0.332^2$  GeV<sup>2</sup>. Column  $\%M$  represents the error of  $M_{\text{th}}$  with respect to  $M_{\text{exp}}$ , according to Eq. (26).

(29). This can be explained, as the data selection scenarios in these references are different from the current study. In these past studies, the scalar meson  $f_0(500)$  was included, which might have caused the slight difference of the slope and the intercept compared to our study.

To connect our results with the mesonic spectroscopy data [68, 72–74] we split the isoscalar states  $f_0$  into two sets. The first set, i.e., set 1, is related to the  $n\bar{n} = (u\bar{u} + d\bar{d})/\sqrt{2}$  states, which are represented by  $f_0(980)$ ,  $f_0(1500)$ ,  $f_0(2020)$  and  $f_0(2200)$ . The second set, i.e., set 2, is related to  $s\bar{s}$  states, also called  $f'_0$ , which is represented by  $f_0(1370)$ ,  $f_0(1710)$ ,  $f_0(2100)$  and  $f_0(2330)$ .

Using the states that belong to set 1 we plot a Chew-Frautschi plane represented as  $n_r \times m^2$ , where  $n_r$  is the spectroscopy radial excitation and  $m^2$  is the squared scalar meson mass represented by the dots (our model) or squares (PDG) in figure 4. Using a standard linear regression method we obtain the experimental and theoretical Regge trajectories for set 1, given by:

$$m_{Exp}^2 = (1.314 \pm 0.017) n_r - (0.285 \pm 0.332), \quad (30)$$

$$m_{th}^2 = (1.288 \pm 0.009) n_r - (0.117 \pm 0.024). \quad (31)$$

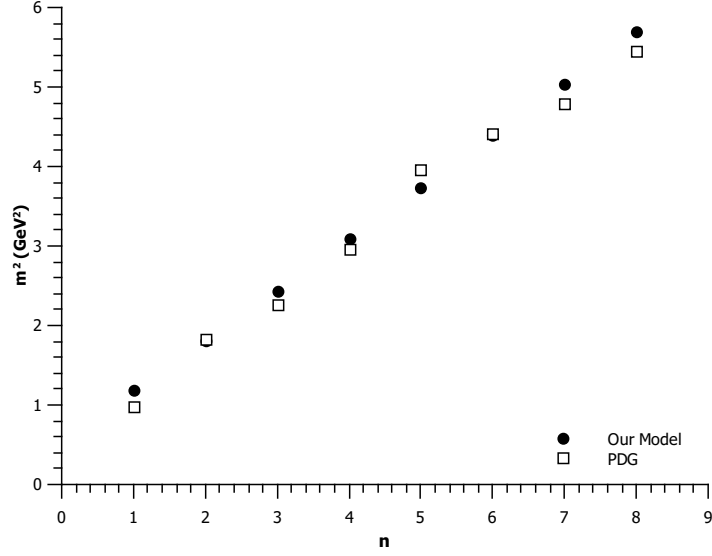


Figure 3. Scalar meson  $f_0$  family squared masses as a function of their holographic radial excitation  $n$  obtained within the deformed  $AdS_5$  space approach (dots) and from PDG (squares), as presented in Table V.

For the states belonging to set 2, we plot Fig. 5 and obtain the experimental and theoretical Regge trajectories, given by:

$$m_{Exp}^2 = (1.236 \pm 0.052) n_r - (0.576 \pm 0.142), \quad (32)$$

$$m_{th}^2 = (1.300 \pm 0.005) n_r - (0.496 \pm 0.012). \quad (33)$$

The Regge trajectories for scalar mesons belonging to the set 1 and 2 from our model, represented by Eqs. (31) and (33), present Regge slopes ranged within the  $1.25 \pm 0.15 \text{ GeV}^2$  which is close to the universal value  $1.1 \text{ GeV}^2$  [72, 75].

## V. HADRONIC SPECTRA FOR VECTOR MESONS

Vector mesons have the same internal structure ( $q\bar{q}$ ) as the scalar mesons, but with total angular momentum  $J = 1$ . They are represented on the boundary theory by the operator:

$$\mathcal{O}_{VM} = \bar{q} \gamma^\mu D_{\{J_1 \dots J_m\}} q \quad \text{with} \quad \sum_{i=1} J_i = J. \quad (34)$$

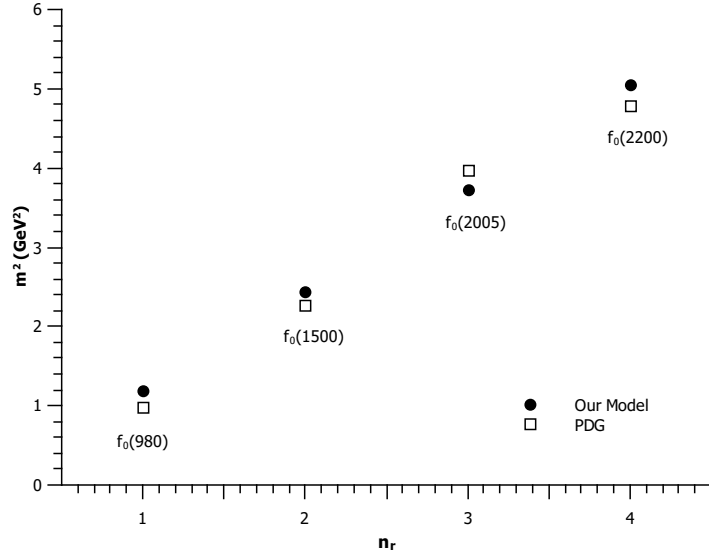


Figure 4. Scalar meson  $f_0 [n\bar{n} = (u\bar{u}+d\bar{d})/\sqrt{2}]$  states belonging to set 1 squared masses as a function of their spectroscopy radial excitation  $n_r$  obtained within the deformed  $AdS_5$  space approach (dots) and coming from PDG (squares).

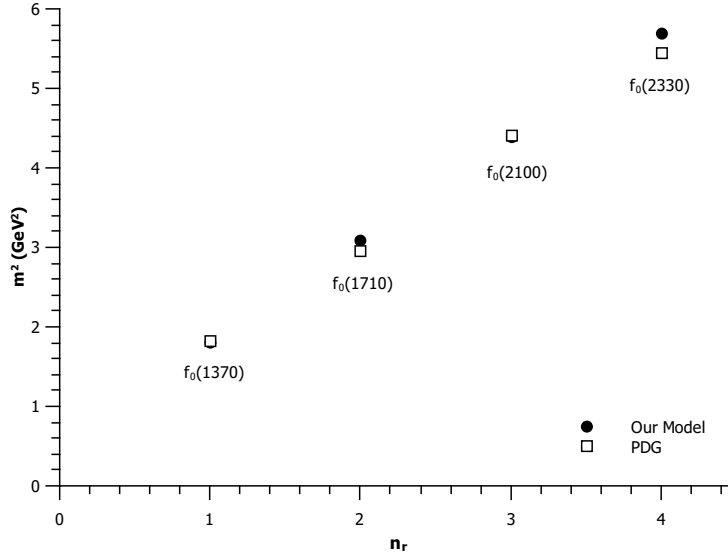


Figure 5. Scalar meson  $f_0[s\bar{s}]$  states belonging to set 2 squared masses as a function of their spectroscopy radial excitation  $n_r$ , obtained within the deformed  $AdS_5$  space approach (dots) and from PDG (squares).

In the holographic description, vector mesons are dual to the massive vector field in the  $AdS_5$ . Hence, the action for a massive vector field is needed, given by:

$$S = -\frac{1}{2} \int d^5x \sqrt{-g} \left[ \frac{1}{2} g^{pm} g^{qn} F_{mn} F_{pq} + M_5^2 g^{pm} A_p A_m \right], \quad (35)$$

where the vector field stress tensor is defined as  $F_{mn} = \partial_m A_n - \partial_n A_m$ .

The equations of motion are achieved by  $\delta S / \delta A_n = 0$ , so that:

$$\partial_z [e^{-B(z)} F_{zn} \eta^{nq}] + \partial_\mu [e^{-B(z)} \eta^{m\mu} F_{mn} \eta^{nq}] - e^{-3B(z)} M_5^2 A_n \eta^{nq} = 0, \quad (36)$$

where  $B(z) = -A(z)$ .

Considering a plane wave ansatz with the amplitude only depending on the  $z$  coordinate and propagating in the transverse coordinates  $x^\mu$  with momentum  $q_\mu$ , we obtain

$$A_\nu(z, x^\mu) = v(z) e^{iq_\mu x^\mu} \epsilon_\nu, \quad (37)$$

assuming  $A_z = 0$  and  $\epsilon^\nu \epsilon_\nu = \eta^{\nu\lambda} \epsilon_\nu \epsilon_\lambda = 1$  is the unitary 4-vector defined in the transverse space to the  $z$  coordinate, with components  $\epsilon_\nu = 1/2(1, 1, 1, 1)$ . We use the fact  $\partial_\mu A^\mu = 0$  which implies  $q^\mu \epsilon_\mu = \eta^{\mu\lambda} q^\mu \epsilon_\lambda = q \cdot \epsilon = 0$  ensuring that the field can be written as a plane wave. Notably that  $F_{zn} = \partial_z A_n$  and  $\eta^{m\mu} \partial_\mu F_{mn} = -q^2 A_n$ . After some algebraic manipulation and defining  $v(z) = \psi(z) e^{\frac{B(z)}{2}}$ , we obtain the ‘Schrödinger-like’ equation, given by:

$$-\psi''(z) + \left[ \frac{B'^2(z)}{4} - \frac{B''(z)}{2} + e^{-2B(z)} M_5^2 \right] \psi(z) = -q^2 \psi(z), \quad (38)$$

where  $E = -q^2$  are eigenenergies.

### A. Results for vector mesons spectra

We consider the case  $J = 1$ . Then, recalling that  $M_5^2 = (\Delta - p)(\Delta + p - 4)$ , and identifying  $M_5$  as the vector meson bulk mass, the index of  $p$ -form as total angular momentum ( $p = J = 1$ ) for the vector meson and  $\Delta$  as the conformal dimension, which is  $\Delta = 3$  as each quark contributes with  $3/2$ . Finally, we rewrite Eq.(38) as:

$$-\psi''(z) + \left[ \frac{B'^2(z)}{4} - \frac{B''(z)}{2} \right] \psi(z) = -q^2 \psi(z), \quad (39)$$

with  $B(z) = -A(z)$  and  $M_5^2 = 0$  for vector mesons.

	Vector meson $\rho (1^+(1^{--}))$			
	$\rho$ meson	$M_{\text{exp}}$ GeV [69]	$M_{\text{th}}$ GeV	% $M$
$n = 1$	$\rho(770)$	$0.77526 \pm 0.00025$	0.868327	12.0422
$n = 2$	$\rho(1450)$	$1.465 \pm 0.025$	1.228	16.1775
$n = 3$	$\rho(1570)$	$1.570 \pm 0.070$	1.50399	4.20467
$n = 4$	$\rho(1700)$	$1.720 \pm 0.020$	1.73665	0.968271
$n = 5$	$\rho(1900)$	$1.909 \pm 0.042$	1.94164	1.70972
$n = 6$	$\rho(2150)$	$2.155 \pm 0.021$	2.12696	1.30123

Table VI. Masses of light unflavored vector meson  $\rho$  ( $S = C = B = 0$ ). Column  $n = 1, 2, 3, \dots$  represents holographic radial excitation of the vector mesons. The ground state is represented by  $n = 1$ . Column  $M_{\text{exp}}$  represents experimental data from PDG [69]. Column  $M_{\text{th}}$  represents masses obtained within the deformed  $AdS_5$  space approach and using Eq.(39) with  $k_{\text{vm}} = -0.613^2$  GeV<sup>2</sup>. Column % $M$  represents the error of  $M_{\text{th}}$  with respect to  $M_{\text{exp}}$ , according to Eq. (26).

Solving Eq. (39) numerically with the warp factor constant  $k$  given by  $k_{\text{vm}} = -0.613^2$  GeV<sup>2</sup>, we obtain the masses compatible with the family of vector meson  $\rho$ , with  $I^G J^{PC} = 1^+(1^{--})$ , as indicated in Table VI. The error presented in the last column of Table VI (% $M$ ) was defined in Eq.(26). We also compute the total r.m.s error defined by Eq. (27). For table VI we obtain  $\delta_{rms} = 7.87\%$ .

Using the data from Table VI we plotted a Chew-Frautschi plane represented as  $n \times m^2$ , where  $n$  is the holographic radial excitation, and  $m^2$  is the squared vector meson mass represented by the dots (our model) or squares (PDG) in Fig. 6. Using a standard linear regression method we obtain the experimental and theoretical Regge trajectories for vector meson  $\rho$ , such that:

$$m_{Exp}^2 = (0.720 \pm 0.076) n - (0.223 \pm 0.302), \quad (40)$$

$$m_{th}^2 = (0.754 \pm 8 \times 10^{-7}) n. \quad (41)$$

We did not include the intercept in Eq. (41), because its value is very close to zero ( $\approx 10^{-18}$ ). Moreover, in Eq. (41), the uncertainty in the slope is very small indicating that this fit is practically a straight line.

The authors of Refs. [70, 71] also computed the masses for the  $\rho$  meson family and derived



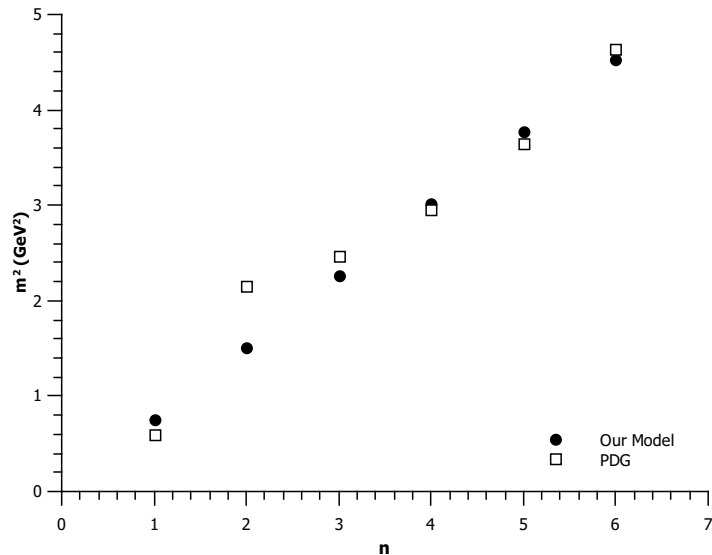


Figure 6. Vector meson  $\rho$  family squared masses as a function of their holographic radial excitation obtained within the deformed  $AdS_5$  space approach (dots) and from PDG (squares), as presented in Table VI.

their Regge trajectories within their holographic softwall model, obtaining approximately the same value for the slope and intercept (considering uncertainties) as the present study, Eq. (41). The data select scenarios in those studies are different from the present study, as they included the vector meson  $\rho(1282)$  as the first radial excited state and excluded the vector meson  $\rho(1570)$ , which the authors argue may be an OZI violating decay of the  $\rho(1700)$ . If we assume the existence of the  $\rho(1282)$  as the first radial excitation ( $n = 2$ ) of the  $\rho$  meson family, then the corresponding percentage error  $\%M$  in Table VI would be smaller and so would the  $\delta_{rms}$  error.

As performed for the scalar mesons, we can resort to the mesonic spectroscopy data [68, 72–74] and note that all vector mesons listed in Table VI are not in the same spectroscopic state, meaning that only  $\rho(770)$ ,  $\rho(1450)$ ,  $\rho(1900)$  and  $\rho(2150)$  belong to the  $S$ -wave represented by  $1^3S_1$ ,  $2^3S_1$ ,  $3^3S_1$  and  $4^3S_1$ , respectively. In this study, we used the spectroscopic notation, such as,  $n_r^{2S+1}L_J$ , where  $n_r$  is the spectroscopy radial excitation. Using these states we plot in a Chew-Frautschi plane represented as  $n_r \times m^2$ , where  $n_r$  is the spectroscopy radial excitation and  $m^2$  is the squared vector meson mass represented by the dots (our model) or squares (PDG) in figure 7. Using a standard linear regression method,

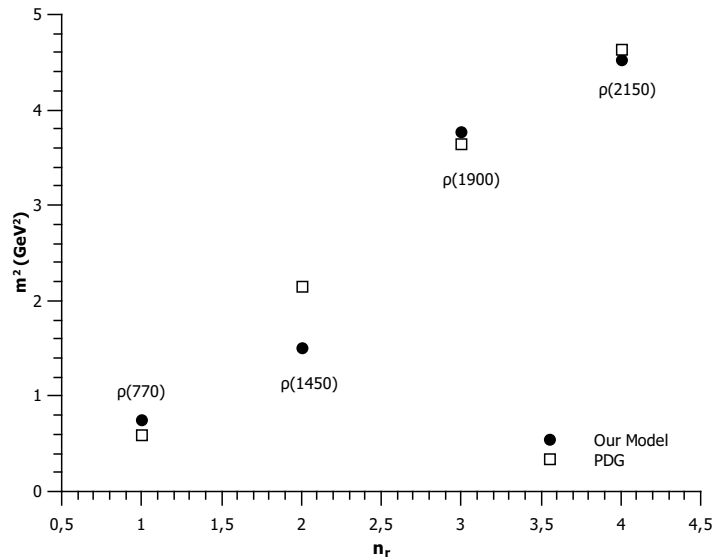


Figure 7. Vector mesons  $\rho$  belonging to  $S$ -wave squared masses as a function of their spectroscopy radial excitation  $n_r$  obtained within the deformed  $AdS_5$  space approach (dots) and from PDG (squares).

we obtain the experimental and theoretical Regge trajectories for vector meson  $\rho$  belonging to the  $S$ -wave, so that:

$$m_{Exp}^2 = (1.363 \pm 0.092) n_r - (0.648 \pm 0.252), \quad (42)$$

$$m_{th}^2 = (1.357 \pm 0.213) n_r - (0.754 \pm 0.584). \quad (43)$$

The Regge trajectory for vector mesons belonging to the  $S$ -wave from our model, represented by Eq. (43), yield a Regge slope in the range  $1.25 \pm 0.15 \text{ GeV}^2$  which is close to the universal value  $1.1 \text{ GeV}^2$  [72, 75].

Furthermore, if we follow the original motivation for the softwall model, it would be natural to suppose that  $k_{sm}$  and  $k_{vm}$  are related to the string tension for the flux tube that connects the two quarks inside the meson. This information is contained in the confining part of the  $q\bar{q}$  potential, and it is in principle a spin independent term. Therefore, in the AdS/QCD models with dilatons in the action, the slope parameter should be universal for scalar and vector mesons, as it happens in the conventional softwall model [16, 49].

Interestingly  $k_{sm}$  and  $k_{vm}$  are related, namely  $3k_{sm} \approx k_{vm}$ . This peculiarity could be attributed to the fact that in the EOM for scalar mesons, Eq.(9), we performed the substi-

tution  $B(z) = -3A(z)$ . On the other hand, in the EOM for vector mesons, Eq.(36), we used  $B(z) = -A(z)$ , leading to  $k_{vm} \approx 3k_{sm}$ .

## VI. HADRONIC SPECTRA FOR BARYONS

Within the quark model, constituent baryons are particles with a semi integer spin formed by a bound state of three valence quarks. In this study, we disregard states of baryons with higher complexity, composed of three quarks added to any number of quark and antiquark pairs, e.g., pentaquark states ( $qqqq\bar{q}$ ). Hence, we use the following description for baryons, such that:

$$|qqq\rangle_A = |\text{color}\rangle_A \otimes |\text{space; spin-flavor}\rangle_S. \quad (44)$$

The three colors are represented by an  $SU(3)$  singlet, without dynamics and completely antisymmetric. The spatial wave function is related to  $O(6)$ , and the spin-flavor wave function is related to  $SU(6)$ . A review on baryon physics is provided in Refs. [76, 77]. In this study we are interested in light baryons composed of  $u$  and  $d$  quarks with a spin of  $1/2$  and with higher spins ( $3/2$  and  $5/2$ ).

Within the holographic description, baryons are dual to the massive spinor fields in  $AdS_5$ . We start our discussion from the free spinor field action without surface terms [78–81]:

$$S = \int_{AdS} d^5x \sqrt{g} \bar{\Psi} (\not{D} - m_5) \Psi. \quad (45)$$

We disregarded the hypersphere  $S^5$ , as for our purposes, the spinor field does not depend on these coordinates. Further, in the action (45),  $g$  is the determinant of the metric of the deformed  $AdS_5$  space, given by Eq. (4).

As we deal with fermions in a curved space, we need to construct a local Lorentz frame or a vielbein. To simplify our notation, we will use  $a, b, c$  to denote indexes in flat space, and  $m, n, p, q$  to denote indexes in curved space (deformed  $AdS_5$  space). The Greek indexes  $\mu, \nu$  are defined in the Minkowski space. Thus, a useful choice is:

$$e_m^a = e^{A(z)} \delta_m^a, \quad e_a^m = e^{-A(z)} \delta_a^m e^{ma} = e^{-A(z)} \eta^{ma}, \quad \text{with} \quad m = 0, 1, 2, 3, 5. \quad (46)$$

The Levi-Civita connection is defined as:

$$\Gamma_{mn}^p = \frac{1}{2} g^{pq} (\partial_n g_{mq} + \partial_m g_{nq} - \partial_q g_{mn}), \quad \text{with} \quad g_{mn} = e^{2A(z)} \eta_{mn}. \quad (47)$$

The corresponding spin connection  $\omega_m^{\mu\nu}$ , is given by:

$$\omega_m^{ab} = e_n^a \partial_m e^{nb} + e_n^a e^{pb} \Gamma_{pm}^n. \quad (48)$$

Because the only non-vanishing  $\Gamma_{mn}^p$  are:

$$\Gamma_{\mu\nu}^5 = A'(z)\eta_{\mu\nu}, \quad \Gamma_{55}^5 = -A'(z) \quad \text{and} \quad \Gamma_{\nu 5}^\mu = -A'(z)\delta_\nu^\mu, \quad (49)$$

we obtain:

$$\omega_\mu^{5\nu} = -\omega_\mu^{\nu 5} = \partial_z A(z)\delta_\mu^\nu, \quad (50)$$

and all other components disappear.

The equations of motion are easily derived from Eq. (45), so that:

$$(\not{D} - m_5)\Psi = 0 \quad \text{and} \quad \bar{\Psi}(-\overleftarrow{\not{D}} - m_5) = 0. \quad (51)$$

Now using (4), (46) and (50), one can write the operator  $\not{D}$  in (51), so that:

$$\not{D} \equiv g^{mn} e_n^a \gamma_a \left( \partial_m + \frac{1}{2} \omega_m^{bc} \Sigma_{bc} \right) = e^{-A(z)} \gamma^5 \partial_5 + e^{-A(z)} \gamma^\mu \partial_\mu + 2A'(z) \gamma^5, \quad (52)$$

where we employed that  $\gamma_a = (\gamma_\mu, \gamma_5)$ ,  $\{\gamma_a, \gamma_b\} = 2\eta_{ab}$ , and  $\Sigma_{\mu 5} = \frac{1}{4} [\gamma_\mu, \gamma_5]$ . Here,  $\gamma_\mu$  are the usual Dirac's gamma matrices.

The first Dirac equation in Eq. (51) assumes the following form:

$$(e^{-A(z)} \gamma^5 \partial_5 + e^{-A(z)} \gamma^\mu \partial_\mu + 2A'(z) \gamma^5 - m_5) \Psi = 0, \quad (53)$$

where  $\partial_5 \equiv \partial_z$ ,  $z$  is the holographic coordinate in the AdS space and  $m_5$  is the fermion bulk mass. Considering a solution that can be decomposed into right- and left-handed chiral components, such as:

$$\Psi(x^\mu, z) = \left[ \frac{1 - \gamma^5}{2} f_L(z) + \frac{1 + \gamma^5}{2} f_R(z) \right] \Psi_{(4)}(x), \quad (54)$$

with  $\Psi_{(4)}(x)$  satisfying the Dirac equation  $(\not{D} - M)\Psi_{(4)}(x) = 0$  on the four-dimensional boundary space. The left and right modes also obey  $\gamma^5 f_{L/R} = \mp f_{L/R}$  and  $\gamma^\mu \partial_\mu f_R = m f_L$ .

Because the Kaluza-Klein modes are dual to the chirality spinors, we expand  $\Psi_{L/R}$ , so that:

$$\Psi_{L/R}(x^\mu, z) = \sum_n f_{L/R}^n(x^\mu) \phi_{L/R}^n(z). \quad (55)$$

Using Eq. (55) with Eq. (54) in Eq. (53) we obtain a set with two coupled equations, such as:

$$(\partial_z + 2A'(z)e^{A(z)} + m_5 e^{A(z)})\phi_L^n(z) = +M_n\phi_R^n(z) \quad (56)$$

and

$$(\partial_z + 2A'(z)e^{A(z)} - m_5 e^{A(z)})\phi_R^n(z) = -M_n\phi_L^n(z). \quad (57)$$

Decoupling Eqs.(56) and (57), and performing the following change of variables

$$\phi_{L/R}(z) = \psi(z)e^{-2e^{A(z)}}, \quad (58)$$

we obtain a Schrödinger-like equation written for both right and left sectors, given by:

$$-\psi_{R/L}''(z) + [m_5^2 e^{2A(z)} \pm m_5 e^{A(z)} A'(z)] \psi_{R/L}(z) = M_n^2 \psi_{R/L}^n(z), \quad (59)$$

where  $M_n$  in Eqs. (59) depicts the four-dimensional fermion mass.

### A. Results for spin 1/2 baryons spectra

Here, we deal with light baryons with spin  $S = 1/2$  formed by  $u$  and  $d$  quarks. To this end, we consider the following operator on the boundary theory:

$$\mathcal{O}_B = qD_{\{\ell_1 \dots D_{\ell_i} q D_{\ell_{i+1}} \dots D_{\ell_m}\} q}; \quad \text{with} \quad \sum_{i=1} \ell_i = L, \quad (60)$$

where  $L$  is the orbital angular momentum. Here we consider only the case  $L = 0$ .

From the AdS/CFT dictionary we find the following relationship for the fermion bulk mass ( $m_5$ ) and its conformal dimension ( $\Delta$ ), so that:

$$|m_5| = \Delta - 2. \quad (61)$$

As each quark  $u$  or  $d$  contributes with  $\Delta = 3/2$ , then the baryon formed by three quarks exhibits  $\Delta = 9/2$  and consequently  $m_5 = 5/2$ .

Replacing  $m_5 = 5/2$  in the Schrödinger-like equation (59) and solving it numerically, with the warp factor constant  $k$  identified as  $k_{1/2} = 0.205^2 \text{ GeV}^2$ , we obtain the masses compatible with the family of  $N$  baryon, with  $I(J^P) = 1/2(1/2^+)$ , as indicated in Table VII. The error presented in last column of Table VII ( $\%M$ ) is defined in Eq.(26). We also compute the total r.m.s error defined by Eq. (27). For Table VII we obtain  $\delta_{rms} = 4.09\%$ .

	Baryons $N(1/2^+)$			
	$N$ baryon	$M_{\text{exp}}$ GeV [69]	$M_{\text{th}}$ GeV	$\%M$
$n = 1$	$N(939)$	$0.93949 \pm 0.00005$	0.98683	5.04
$n = 2$	$N(1440)$	1.360 to 1.380	1.264	7.76
$n = 3$	$N(1710)$	1.680 to 1.720	1.531	9.94
$n = 4$	$N(1880)$	1.820 to 1.900	1.791	3.70
$n = 5$	$N(2100)$	2.050 to 2.150	2.046	2.58
$n = 6$	$N(2300)$	$2.300^{+0.006}_{-0.005} \ ^{+0.1}_{-0}$	2.296	0.19

Table VII. Masses of  $N(1/2^+)$  baryons. Column  $n = 1, 2, 3, \dots$  represents holographic radial excitation. The ground state is represented by  $n = 1$ . Column  $M_{\text{exp}}$  represents experimental data from PDG [69]. Column  $M_{\text{th}}$  represents the masses of  $N(1/2^+)$  baryons with  $k_{1/2} = 0.205^2 \text{ GeV}^2$ , obtained within the deformed  $AdS_5$  space approach and using Eq.(59). Column  $\%M$  represents the error of  $M_{\text{th}}$  with respect to  $M_{\text{exp}}$ , according to Eq. (26).

Using the data from Table VII, we plotted a Chew-Frautschi plane represented as  $n \times m^2$ , where  $n$  is the holographic radial excitation and  $m^2$  is the squared  $N(1/2^+)$  baryon mass represented by the dots (our model) or squares (PDG) in Fig. 8. Using a standard linear regression method, we obtain the experimental and theoretical Regge trajectories for the  $N(1/2^+)$  baryon, such that:

$$m_{Exp}^2 = (0.863 \pm 0.029) n + (0.114 \pm 0.111), \quad (62)$$

$$m_{th}^2 = (0.860 \pm 0.042) n - (0.081 \pm 0.164). \quad (63)$$

As performed for the scalar and vector mesons we resort to baryonic spectroscopy and attempt to recognize which baryons among those listed in Table VII belong to the same spectroscopy state. According to Refs. [76, 77], we see that the states  $N(939)$ ,  $N(1440)$ ,  $N(1710)$  and  $N(2100)$  belong to the state  $D_L \equiv (56, {}^2 8)_0$  with spectroscopy radial excitation  $n_r$ , corresponding to  $n_r = 1, 2, 3, 4$ , respectively, with orbital angular momentum  $L = 0$ . In this notation,  $D$  represents the 56-plet, which can be broken into an octet with spin  $1/2$  ( ${}^2 8$ ) and a decuplet with spin  $3/2$  ( ${}^4 10$ ). For these mentioned states, we plot a Chew-Frautschi plane represented as  $n_r \times m^2$ , where  $n_r$  is the spectroscopy radial excitation and  $m^2$  is the squared  $N(1/2^+)$  baryon mass belonging to the  $(56, {}^2 8)_0$  state represented by the dots (our

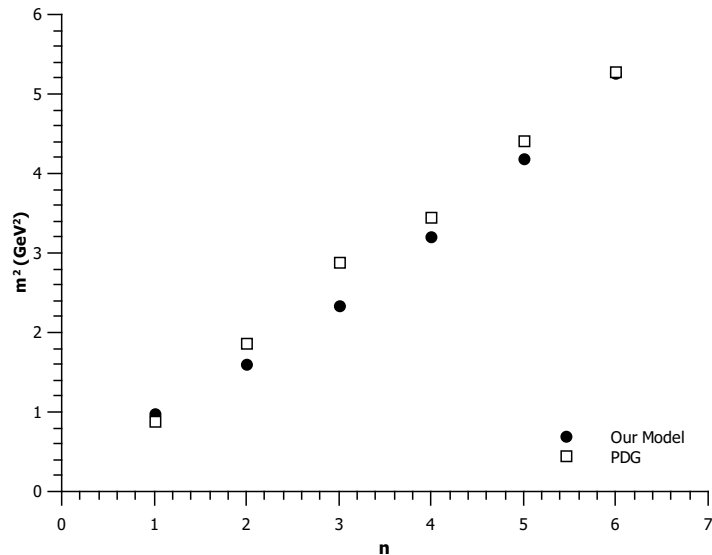


Figure 8.  $N(1/2^+)$  baryon family squared masses as a function of their holographic radial excitation obtained within the deformed  $AdS_5$  space approach (dots) and from PDG (squares), as presented in Table VII.

model) or squares (PDG) in Fig. 9. Using a standard linear regression method, we obtain the experimental and theoretical Regge trajectories for  $N(1/2^+)$  baryon in the  $(56,^2 8)_0$  state, so that:

$$m_{Exp}^2 = (1.160 \pm 0.090) n_r - (0.384 \pm 0.246), \quad (64)$$

$$m_{th}^2 = (1.038 \pm 0.204) n_r - (0.320 \pm 0.560). \quad (65)$$

The Regge trajectory for the  $N(1/2^+)$  baryon belonging to the same multiplet comes from our model, represented by Eq. (65), and presents a Regge slope in the range  $1.081 \pm 0.036$   $\text{GeV}^2$  which is close to the universal value  $1.1 \text{ GeV}^2$  [82].

## B. Results for higher spin baryons spectra

Here, we deal with light baryons, according to the same structure as in the previous section and a higher spin, meaning, e.g.,  $S = 3/2$  or  $S = 5/2$ . To this end, we employ the same approach for the higher spin glueball as in Subsection III A. To obtain the spectrum for spin  $3/2$  baryons we insert symmetrized covariant derivatives in the operator  $\mathcal{O}_B$ , given by Eq. (60). Then, the conformal dimensions related to the spin  $3/2$  baryons is now

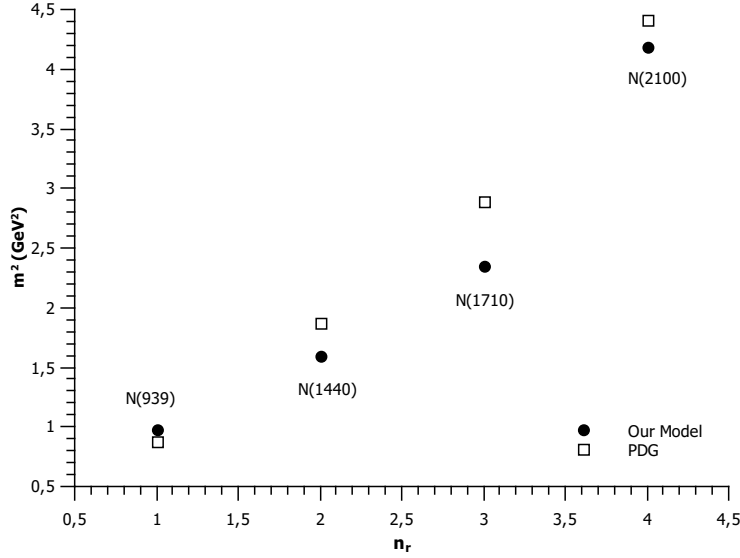


Figure 9.  $N(1/2^+)$  baryons belonging to the  $(56,^2 8)_0$  state squared masses as a function of their spectroscopy radial excitation  $n_r$  obtained within the deformed  $AdS_5$  space approach (dots) and from PDG (squares).

	Baryons $N(3/2^+)$			
	$N$ baryon	$M_{\text{exp}}$ GeV [69]	$M_{\text{th}}$ GeV	$\%M$
$n = 1$	$N(1720)$	1.660 to 1.690	1.326	23.05%
$n = 2$	$N(1900)$	1.900 to 1.940	1.606	12.27%
$n = 3$	$N(2040)$	$2.040^{+0.003}_{-0.004} \pm 0.025$	1.878	8.72%

Table VIII. Masses of  $N(3/2^+)$  baryons. Column  $n = 1, 2, 3, \dots$  represents holographic radial excitation. The ground state is represented by  $n = 1$ . Column  $M_{\text{exp}}$  represents experimental data from PDG [69]. Column  $M_{\text{th}}$  represents the masses of  $N(3/2^+)$  baryons with  $k_{3/2} = 0.205^2 \text{ GeV}^2$ , obtained within the deformed  $AdS_5$  space approach and using Eq.(59). Column  $\%M$  represents the error of  $M_{\text{th}}$ , according to Eq. (26).

$\Delta_{3/2} = 11/2$ , with  $m_5 = 7/2$ . Solving Eq. (59) with the warp factor constant  $k$  given by  $k_{3/2} = 0.205^2 \text{ GeV}^2$ , we obtain the masses compatible with the family of  $N$  baryon, with  $I(J^P) = 1/2(3/2^+)$ , as indicated in Table VIII. The error presented in last column of table VIII ( $\%M$ ) is defined in Eq.(26). We also compute the total r.m.s error defined by Eq. (27). For Table IX one finds  $\delta_{rms} = 9.00\%$ .



	Baryons $N(3/2^+)$			
	$N$ baryon	$M_{\text{exp}}$ GeV [69]	$M_{\text{th}}$ GeV	$\%M$
$n = 1$			1.326	
$n = 2$	$N(1720)$	1.660 to 1.690	1.606	4.14
$n = 3$	$N(1900)$	1.900 to 1.940	1.878	2.19
$n = 4$	$N(2040)$	$2.040^{+0.003}_{-0.004} \pm 0.025$	2.144	5.09

Table IX. Masses of  $N(3/2^+)$  baryons. Column  $n = 1, 2, 3, \dots$  represents holographic radial excitation. The ground state is represented by  $n = 1$ . Column  $M_{\text{exp}}$  represents experimental data from PDG [69]. Column  $M_{\text{th}}$  represents the masses of  $N(3/2^+)$  baryons with  $k_{3/2} = 0.205^2 \text{ GeV}^2$ , obtained within the deformed  $AdS_5$  space approach and using Eq.(59). Column  $\%M$  represents the error of  $M_{\text{th}}$  with respect to  $M_{\text{exp}}$ , according to Eq. (26). In the first line, we present a possible baryon prediction within our model.

Observing the column ( $\%M$ ) in Table VIII, The errors between  $M_{\text{exp}}$  and  $M_{\text{th}}$  are excessively high, especially for  $n = 1$  and  $n = 2$  states. A possible reinterpretation would be a missing state, which represents the ground state for the  $N(3/2^+)$  baryons family. Taking into account this assumption, regarding a possible missing state, we can reinterpret Table VIII as in Table IX, where in the first line we present a possible baryon prediction obtained within the deformed AdS model. The error presented in last column of table IX ( $\%M$ ) is defined in Eq.(26), We also compute the total r.m.s error defined by Eq. (27). For table IX we find  $\delta_{rms} = 2.13\%$ . We excluded our prediction of the errors calculation. The error in Table VIII are greater than in Table IX. However, this possible ground state  $N(1330)$  that we are reinterpreting is not found in PDG. In PDG the  $\Delta^+$  states with  $J^P = 3/2^+$  and mass around 1320 MeV, is found; hence, our model is possibly not capable to distinguishing these two states. This first state could be  $\Delta(1232)$  as both trajectories,  $\Delta$  and  $N(3/2^+)$ , are supposed to be degenerate in the chiral limit, as it happens with mesons  $\rho$  and  $\omega$ .

Using the data from Table IX we plotted a Chew-Frautschi plane represented as  $n \times m^2$ , where  $n$  is the holographic radial excitation and  $m^2$  is the squared  $N(3/2^+)$  baryon mass represented by the dots (our model), by the triangle (our model prediction) or squares (PDG) in Fig. 10. Using a standard linear regression method we obtain the experimental

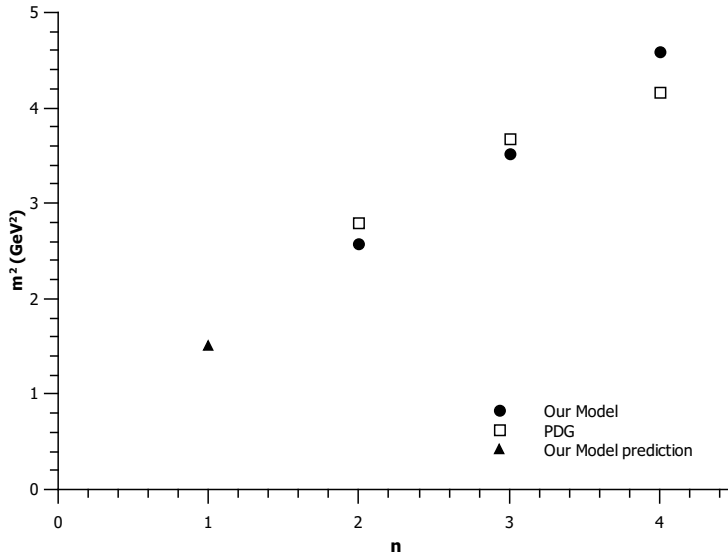


Figure 10.  $N(3/2^+)$  baryon family squared masses as a function of their holographic radial excitation obtained within the deformed  $AdS_5$  space approach (dots), our model prediction (triangle) and from PDG (squares), as presented in Table IX.

and theoretical Regge trajectories for  $N(3/2^+)$  baryons, so that:

$$m_{Exp}^2 = (0.678 \pm 0.117) n + (1.517 \pm 0.364), \quad (66)$$

$$m_{th}^2 = (1.021 \pm 0.017) n + (0.501 \pm 0.047). \quad (67)$$

For the linear fit in Eq.(67) we took into account our predicted state.

The Regge trajectory for the  $N(3/2^+)$  baryon family from our model, represented by Eq. (67), present a Regge slope in the range  $1.081 \pm 0.036 \text{ GeV}^2$  which is close to the universal value  $1.1 \text{ GeV}^2$  [82].

At this point, we deal with baryons of spin  $5/2$ . To this end, once again, insert one more symmetrized covariant derivative in the operator  $\mathcal{O}_B$  given by Eq. (60). Then, we obtain the conformal dimension, given by  $\Delta_{5/2} = 13/2$ , which provides  $m_5 = 9/2$ . Solving Eq. (59) with the warp factor constant  $k$  given by  $k_{5/2} = 0.190^2 \text{ GeV}^2$ , we obtain the masses compatible with the family of  $N$  baryons, with  $I(J^P) = 1/2(5/2^+)$ , as indicated in Table X. The error presented in the last column of table X ( $\%M$ ) is defined in Eq. (26). We compute the total r.m.s error defined by Eq. (27). For Table X one finds  $\delta_{rms} = 2.76\%$ .

From Table X, we plotted a Chew-Frautschi plane as  $n \times m^2$ , where  $n$  is the holographic

	Baryons $N(5/2^+)$			
	$N$ baryon	$M_{\text{exp}}$ GeV [69]	$M_{\text{th}}$ GeV	$\%M$
$n = 1$	$N(1680)$	1.665 to 1.680	1.542	7.78
$n = 2$	$N(1860)$	$1.830^{+120}_{-60}$	1.804	1.44
$n = 3$	$N(2000)$	$2.090 \pm 120$	2.059	1.49

Table X. Masses of  $N(5/2^+)$  baryons. Column  $n = 1, 2, 3, \dots$  represents holographic radial excitation. The ground state is represented by  $n = 1$ . Column  $M_{\text{exp}}$  represents experimental data from PDG [69]. Column  $M_{\text{th}}$  represents the masses of  $N(5/2^+)$  baryons with  $k_{5/2} = 0.190^2 \text{ GeV}^2$ , obtained within the deformed  $AdS_5$  space approach and using Eq.(59). Column  $\%M$  represents the error of  $M_{\text{th}}$  with respect to  $M_{\text{exp}}$ , according to Eq. (26).

radial excitation and  $m^2$  is the squared  $N(5/2^+)$  baryon mass represented by the dots (our model) or squares (PDG) in figure 11. Using a standard linear regression method we obtain the experimental and theoretical Regge trajectories for  $N(5/2^+)$  baryons, so that:

$$m_{Exp}^2 = (0.785 \pm 0.135) n + (1.934 \pm 0.291), \quad (68)$$

$$m_{th}^2 = (0.931 \pm 0.031) n + (1.429 \pm 0.068). \quad (69)$$

The Regge trajectory for the  $N(5/2^+)$  baryon family from our model, represented by Eq. (69), present a Regge slope near the range  $1.081 \pm 0.036 \text{ GeV}^2$  which is close to the universal value  $1.1 \text{ GeV}^2$  [82].

Notably, the numeric values of the warp factor constant  $k$  for the baryons in this study are approximately independent of their spin, meaning that  $k_{1/2} = k_{3/2} \approx k_{5/2}$ .

## VII. SUMMARY AND CONCLUSIONS

We studied the hadronic spectra based on the holographic model within deformed  $AdS_5$  space metrics, establishing that the warp factor is  $A(z) = -\log(z) + kz^2/2$  instead of  $A(z) = -\log(z)$  of the pure AdS space. This deformation implies that there is no dilaton field in the action as in the original softwall model. In our model, different values are needed for the parameter  $k$  for each particle sector. A possible interpretation for this behavior is the following: if one assumes that the QCD vacuum is defined by the metric, our result

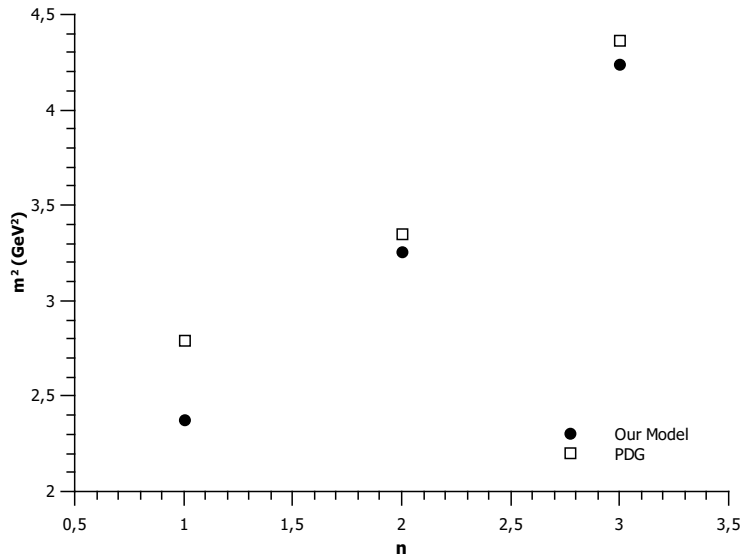


Figure 11.  $N(5/2^+)$  baryon family squared masses as a function of their holographic radial excitation obtained within the deformed  $AdS_5$  space approach (dots) and from PDG (squares), as presented in Table X.

of multiple values of  $k$  indicates that the QCD vacuum should be non-trivial and possibly composed of various non-equivalent vacua states.

The main achievement of this study is to provide an approach that can adequately accommodate the spectra for even and odd glueballs, scalar ( $0^+(0^{++})$ ) and vector mesons ( $1^+(1^{--})$ ), as well as  $N$  baryons with spin  $1/2$ ,  $3/2$  and  $5/2$  using the same holographic approach. This implies that the masses of these mentioned particles, computed using our model, and the derived Regge trajectories are in agreement with the literature.

For the even and odd glueball cases, our model provides appropriate masses, as indicated in Tables I and II, when compared with other approaches (a summary of even and odd spin glueball masses obtained from lattice and other models, is given in Tables III and IV). The computed masses for higher even and odd spin glueballs were placed in a Chew-Frautschi plane  $m^2 \times J$ . We derived the Regge trajectories related to the pomeron and the odderon which are likewise in agreement with the literature.

Our model performs well for scalar mesons, providing appropriate masses for the  $f_0$  ( $0^+(0^{++})$ ), as indicated in Table V, as compared with the data from PDG [69]. The obtained Regge trajectory from  $m^2 \times n$  is compatible with the one of the holographic softwall model

[70, 71]. Using spectroscopy data for the scalar mesons, we split them into two sets. The first one contains only  $n\bar{n} = 1/\sqrt{2}(u\bar{u} + d\bar{d})$ , while the second contains only  $s\bar{s}$ . For these sets, we derived Regge trajectories in  $m^2 \times n_r$  and found that they are compatible with the literature [72, 75].

For the vector meson  $\rho(1^+(1^{--}))$  our model provided appropriate masses as well, as shown in Table VI compared with PDG. The obtained Regge trajectory from  $m^2 \times n$  is compatible with the one from the holographic softwall model [70, 71]. Using the spectroscopy data for the vector mesons, we selected the  $S$ -wave states and derived their Regge trajectory in  $m^2 \times n_r$  finding agreement with the literature [72, 75].

Our model also provides appropriate masses for the  $N(1/2^+)$  baryon, as shown in Table VII, compared with PDG. In this case, we likewise used the baryonic spectroscopic data to select states in the same multiplet, only varying their radial excitation. From these states we derived the Regge trajectory, which was compatible with the literature [82].

For the  $N(3/2^+)$  baryon, we obtained unsatisfactory results for the masses as shown in Table VIII. These results can be improved by introducing a hypothetical baryonic state to occupy the ground state (Table IX). Using this assumption, the errors decrease and the derived Regge trajectory is compatible with the literature [82].

Finally, for the  $N(5/2^+)$  baryon our model provides appropriate masses, as shown in Table X, in comparison with PDG, and the Regge trajectory is in a reasonable agreement with the literature [82].

It is important to note that in our model, the form of the warp factor is the same for all studied particles, whereas the parameter  $k$  is adjusted for each case. In ref. [29] the authors employ different warp factors for each kind of particle that is dependent on the angular momentum. In our case, for even and odd glueballs, the value of  $k$  is the same,  $k_{gbe} = k_{gbo} = 0.31^2 \text{ GeV}^2$ . For scalar and vector mesons, we found that  $k_{vm} \approx 3k_{sm}$ , as discussed at the end of Subsection V A. For the baryonic case, we found  $k_{1/2} = k_{3/2} \approx k_{5/2}$ .

The Regge trajectories presented in this study related to hadronic spectroscopy for scalar mesons (31), (33), vector mesons (43), and baryons (65), (67), (69) point towards a universal Regge slope around  $1.1 \text{ GeV}^2$  in accordance with the literature [72, 75, 82, 83].

Our model finds different signs in the exponential of the warp factor, depending on each hadronic sector. Hence the question regarding the sign of the dilaton in the original softwall model persists. Despite the different signs for different sectors, we have no massless fields

in our model. This a consequence of the deformed geometry instead of the introduction of a dilaton field in the action as in the original softwall model.

## ACKNOWLEDGMENTS

The authors would like to thank Carlos Alfonso Ballon Bayona for useful discussions, and Oleg Andreev and Song He for useful correspondence. H.B-F. would like to thank partial financial support from Conselho Nacional de Desenvolvimento Científico e Tecnológico (CNPq) and Coordenação de Aperfeiçoamento de Pessoal de Nível Superior (Capes) (Brazilian Agencies). A. V. and M. A. M. C. would like to thank the financial support given by FONDECYT (Chile) under Grants No. 1180753 and No. 3180592 respectively. D.L. is supported by the National Natural Science Foundation of China (11805084), the PhD Start-up Fund of Natural Science Foundation of Guangdong Province (2018030310457) and Guangdong Pearl River Talents Plan (2017GC010480).

- 
- [1] J. M. Maldacena, “The Large N limit of superconformal field theories and supergravity,” *Adv. Theor. Math. Phys.* **2**, 231 (1998) [hep-th/9711200].
  - [2] S. S. Gubser, I. R. Klebanov and A. M. Polyakov, “Gauge theory correlators from noncritical string theory,” *Phys. Lett. B* **428**, 105 (1998) [hep-th/9802109].
  - [3] E. Witten, “Anti-de Sitter space and holography,” *Adv. Theor. Math. Phys.* **2**, 253 (1998) [hep-th/9802150].
  - [4] E. Witten, “Anti-de Sitter space, thermal phase transition, and confinement in gauge theories,” *Adv. Theor. Math. Phys.* **2**, 505 (1998) [hep-th/9803131].
  - [5] O. Aharony, S. S. Gubser, J. M. Maldacena, H. Ooguri and Y. Oz, “Large N field theories, string theory and gravity,” *Phys. Rept.* **323**, 183 (2000) [hep-th/9905111].
  - [6] J. Polchinski and M. J. Strassler, “Hard scattering and gauge / string duality,” *Phys. Rev. Lett.* **88**, 031601 (2002) [hep-th/0109174].
  - [7] H. Boschi-Filho and N. R. F. Braga, “Gauge / string duality and scalar glueball mass ratios,” *JHEP* **0305**, 009 (2003) [hep-th/0212207].
  - [8] H. Boschi-Filho and N. R. F. Braga, “QCD / string holographic mapping and glueball mass

- spectrum,” *Eur. Phys. J. C* **32**, 529 (2004) [hep-th/0209080].
- [9] J. Erlich, E. Katz, D. T. Son and M. A. Stephanov, “QCD and a holographic model of hadrons,” *Phys. Rev. Lett.* **95**, 261602 (2005) [hep-ph/0501128].
- [10] L. Da Rold and A. Pomarol, “Chiral symmetry breaking from five dimensional spaces,” *Nucl. Phys. B* **721**, 79 (2005) [hep-ph/0501218].
- [11] G. F. de Teramond and S. J. Brodsky, “Hadronic spectrum of a holographic dual of QCD,” *Phys. Rev. Lett.* **94**, 201601 (2005) [hep-th/0501022].
- [12] L. Da Rold and A. Pomarol, “The Scalar and pseudoscalar sector in a five-dimensional approach to chiral symmetry breaking,” *JHEP* **0601**, 157 (2006) [hep-ph/0510268].
- [13] A. Pomarol and A. Wulzer, “Baryon Physics in Holographic QCD,” *Nucl. Phys. B* **809**, 347 (2009) [arXiv:0807.0316 [hep-ph]].
- [14] C. Wang, S. He, M. Huang, Q. S. Yan and Y. Yang, “Scalar Mesons and glueballs in Dp-Dq hard-wall models,” *Chin. Phys. C* **34**, 319 (2010) [arXiv:0902.0864 [hep-ph]].
- [15] Z. Li and B. Q. Ma, “Baryon spectrum in a finite-temperature AdS/QCD model,” *Phys. Rev. D* **89**, no. 1, 015014 (2014) [arXiv:1312.3451 [hep-ph]].
- [16] A. Karch, E. Katz, D. T. Son and M. A. Stephanov, “Linear confinement and AdS/QCD,” *Phys. Rev. D* **74**, 015005 (2006) [hep-ph/0602229].
- [17] S. He, M. Huang, Q. S. Yan and Y. Yang, “Confront Holographic QCD with Regge Trajectories,” *Eur. Phys. J. C* **66**, 187 (2010) [arXiv:0710.0988 [hep-ph]].
- [18] A. Vega and I. Schmidt, “Hadrons in AdS/QCD correspondence,” *Phys. Rev. D* **79**, 055003 (2009) [arXiv:0811.4638 [hep-ph]].
- [19] T. Branz, T. Gutsche, V. E. Lyubovitskij, I. Schmidt and A. Vega, “Light and heavy mesons in a soft-wall holographic approach,” *Phys. Rev. D* **82**, 074022 (2010) [arXiv:1008.0268 [hep-ph]].
- [20] T. Gutsche, V. E. Lyubovitskij, I. Schmidt and A. Vega, “Dilaton in a soft-wall holographic approach to mesons and baryons,” *Phys. Rev. D* **85**, 076003 (2012) [arXiv:1108.0346 [hep-ph]].
- [21] S. S. Afonin, “Generalized Soft Wall Model,” *Phys. Lett. B* **719**, 399 (2013) [arXiv:1210.5210 [hep-ph]].
- [22] Z. Fang, D. Li and Y. L. Wu, “IR-improved Soft-wall AdS/QCD Model for Baryons,” *Phys. Lett. B* **754**, 343 (2016) [arXiv:1602.00379 [hep-ph]].
- [23] S. Cortés, M. Á. Martín Contreras and J. R. Roldán, *Phys. Rev. D* **96**, no. 10, 106002 (2017) [arXiv:1706.09502 [hep-ph]].

- [24] M. Á. Martín Contreras, A. Vega and S. Cortés, “Light Pseudoscalar and Axial Spectroscopy using AdS/QCD Modified Soft Wall Model,” arXiv:1811.10731 [hep-ph].
- [25] S. S. Afonin and A. D. Katanaeva, “Glueballs and deconfinement temperature in AdS/QCD,” Phys. Rev. D **98**, no. 11, 114027 (2018) [arXiv:1809.07730 [hep-ph]].
- [26] T. Gutsche, V. E. Lyubovitskij, I. Schmidt and A. Y. Trifonov, “Mesons in a soft-wall AdS-Schwarzschild approach at low temperature,” arXiv:1902.01312 [hep-ph].
- [27] O. Andreev, “ $1/q^{*2}$  corrections and gauge/string duality,” Phys. Rev. D **73**, 107901 (2006) [hep-th/0603170].
- [28] O. Andreev and V. I. Zakharov, “Heavy-quark potentials and AdS/QCD,” Phys. Rev. D **74**, 025023 (2006) [hep-ph/0604204].
- [29] H. Forkel, M. Beyer and T. Frederico, “Linear square-mass trajectories of radially and orbitally excited hadrons in holographic QCD,” JHEP **0707**, 077 (2007) [arXiv:0705.1857 [hep-ph]].
- [30] C. D. White, “The Cornell potential from general geometries in AdS / QCD,” Phys. Lett. B **652**, 79 (2007) [hep-ph/0701157].
- [31] R. C. L. Bruni, E. Folco Capossoli and H. Boschi-Filho, “Quark-antiquark potential from a deformed AdS/QCD,” Adv. High Energy Phys. **2019**, 1901659 (2019) [arXiv:1806.05720 [hep-th]].
- [32] M. Rinaldi and V. Vento, Eur. Phys. J. A **54**, 151 (2018) doi:10.1140/epja/i2018-12600-9 [arXiv:1710.09225 [hep-ph]].
- [33] G. F. de Teramond and S. J. Brodsky, “Light-Front Holography and Gauge/Gravity Duality: The Light Meson and Baryon Spectra,” Nucl. Phys. Proc. Suppl. **199**, 89 (2010) doi:10.1016/j.nuclphysbps.2010.02.010 [arXiv:0909.3900 [hep-ph]].
- [34] F. Zuo, “Improved Soft-Wall model with a negative dilaton,” Phys. Rev. D **82**, 086011 (2010) doi:10.1103/PhysRevD.82.086011 [arXiv:0909.4240 [hep-ph]].
- [35] S. Nicotri, “Phenomenology Of The Holographic Soft-Wall Model Of QCD With ‘Reversed’ Dilaton,” AIP Conf. Proc. **1317**, no. 1, 322 (2010) doi:10.1063/1.3536578 [arXiv:1009.4829 [hep-ph]].
- [36] A. Karch, E. Katz, D. T. Son and M. A. Stephanov, “On the sign of the dilaton in the soft wall models,” JHEP **1104**, 066 (2011) [arXiv:1012.4813 [hep-ph]].
- [37] S. Dobbs, A. Tomaradze, T. Xiao and K. K. Seth, “Comprehensive Study of the Radiative Decays of  $J/\psi$  and  $\psi(2S)$  to Pseudoscalar Meson Pairs, and Search for Glueballs,” Phys. Rev.



- D **91**, no. 5, 052006 (2015) [arXiv:1502.01686 [hep-ex]].
- [38] H. Fritzsche and M. Gell-Mann, “Current algebra: Quarks and what else?,” eConf C **720906V2**, 135 (1972) [hep-ph/0208010].
- [39] C. Augier *et al.* [UA4/2 Collaboration], “A Precise measurement of the real part of the elastic scattering amplitude at the S anti-p p S,” Phys. Lett. B **316**, 448 (1993).
- [40] R. Avila, P. Gauron and B. Nicolescu, “How can the Odderon be detected at RHIC and LHC,” Eur. Phys. J. C **49**, 581 (2007) [hep-ph/0607089].
- [41] M. Ablikim *et al.* [BES Collaboration], “Partial wave analyses of  $J/\psi \rightarrow \gamma \pi^+ \pi^-$  and  $\gamma \pi^0 \pi^0$ ,” Phys. Lett. B **642**, 441 (2006) [hep-ex/0603048].
- [42] J. Z. Bai *et al.* [BES Collaboration], “Partial wave analyses of  $J/\psi \rightarrow \gamma K^+ K^-$  and  $\gamma K_0(S) K_0(S)$ ,” Phys. Rev. D **68**, 052003 (2003) [hep-ex/0307058].
- [43] C. J. Morningstar and M. J. Peardon, “The Glueball spectrum from an anisotropic lattice study,” Phys. Rev. D **60**, 034509 (1999) [hep-lat/9901004].
- [44] H. B. Meyer and M. J. Teper, “Glueball Regge trajectories and the pomeron: A Lattice study,” Phys. Lett. B **605**, 344 (2005) [hep-ph/0409183].
- [45] Y. Chen, A. Alexandru, S. J. Dong, T. Draper, I. Horvath, F. X. Lee, K. F. Liu and N. Mathur *et al.*, “Glueball spectrum and matrix elements on anisotropic lattices,” Phys. Rev. D **73**, 014516 (2006) [hep-lat/0510074].
- [46] B. Lucini and M. Teper, “SU(N) gauge theories in four-dimensions: Exploring the approach to  $N = \infty$ ,” JHEP **0106**, 050 (2001) [hep-lat/0103027].
- [47] A. P. Szczepaniak and E. S. Swanson, “The Low lying glueball spectrum,” Phys. Lett. B **577**, 61 (2003)[hep-ph/0308268].
- [48] V. Mathieu, F. Buisseret and C. Semay, “Gluons in glueballs: Spin or helicity?,” Phys. Rev. D **77**, 114022 (2008)[arXiv:0802.0088 [hep-ph]].
- [49] P. Colangelo, F. De Fazio, F. Jugeau and S. Nicotri, “On the light glueball spectrum in a holographic description of QCD,” Phys. Lett. B **652** (2007) 73 [hep-ph/0703316].
- [50] H. Boschi-Filho, N. R. F. Braga and H. L. Carrion, “Glueball Regge trajectories from gauge/string duality and the Pomeron,” Phys. Rev. D **73**, 047901 (2006) [hep-th/0507063].
- [51] E. F. Capossoli and H. Boschi-Filho, “Odd spin glueball masses and the Odderon Regge trajectories from the holographic hardwall model,” Phys. Rev. D **88**, no. 2, 026010 (2013) [arXiv:1301.4457 [hep-th]].

- [52] D. M. Rodrigues, E. Folco Capossoli and H. Boschi-Filho, “Twist Two Operator Approach for Even Spin Glueball Masses and Pomeron Regge Trajectory from the Hardwall Model,” *Phys. Rev. D* **95**, no. 7, 076011 (2017) [arXiv:1611.03820 [hep-th]].
- [53] H. Boschi-Filho, N. R. F. Braga, F. Jugeau and M. A. C. Torres, “Anomalous dimensions and scalar glueball spectroscopy in AdS/QCD,” *Eur. Phys. J. C* **73**, 2540 (2013) [arXiv:1208.2291 [hep-th]].
- [54] D. Li and M. Huang, “Dynamical holographic QCD model for glueball and light meson spectra,” *JHEP* **1311**, 088 (2013) [arXiv:1303.6929 [hep-ph]].
- [55] E. Folco Capossoli and H. Boschi-Filho, “Glueball spectra and Regge trajectories from a modified holographic softwall model,” *Phys. Lett. B* **753**, 419 (2016) [arXiv:1510.03372 [hep-ph]].
- [56] E. Folco Capossoli, D. Li and H. Boschi-Filho, “Pomeron and Odderon Regge Trajectories from a Dynamical Holographic Model,” *Phys. Lett. B* **760**, 101 (2016) [arXiv:1601.05114 [hep-ph]].
- [57] E. Folco Capossoli, D. Li and H. Boschi-Filho, “Dynamical corrections to the anomalous holographic soft-wall model: the pomeron and the odderon,” *Eur. Phys. J. C* **76**, no. 6, 320 (2016) [arXiv:1604.01647 [hep-ph]].
- [58] D. M. Rodrigues, E. Folco Capossoli and H. Boschi-Filho, “Scalar and higher even spin glueball masses from an anomalous modified holographic model,” *EPL* **122**, no. 2, 21001 (2018) [arXiv:1611.09817 [hep-ph]].
- [59] A. Donnachie and P. V. Landshoff, “Dynamics of Elastic Scattering,” *Nucl. Phys. B* **267**, 690 (1986).
- [60] S. Donnachie, H. G. Dosch, O. Nachtmann and P. Landshoff, “Pomeron physics and QCD,” *Camb. Monogr. Part. Phys. Nucl. Phys. Cosmol.* **19**, 1 (2002).
- [61] C. Csaki, H. Ooguri, Y. Oz and J. Terning, “Glueball mass spectrum from supergravity,” *JHEP* **9901**, 017 (1999) [hep-th/9806021].
- [62] R. C. Brower, S. D. Mathur and C. I. Tan, “Glueball spectrum for QCD from AdS supergravity duality,” *Nucl. Phys. B* **587**, 249 (2000) [hep-th/0003115].
- [63] F. J. Llanes-Estrada, P. Bicudo and S. R. Cotanch, “Oddballs and a low odderon intercept,” *Phys. Rev. Lett.* **96**, 081601 (2006) [hep-ph/0507205].
- [64] H. B. Meyer, “Glueball Regge trajectories, PhD. Thesis, University of Oxford”, [hep-lat/0508002].
- [65] A. B. Kaidalov and Y. .A. Simonov, “Glueball spectrum and the Pomeron in the Wilson loop

- approach,” Phys. Atom. Nucl. **63**, 1428 (2000) [Yad. Fiz. **63**, 1428 (2000)] [hep-ph/9911291].
- [66] A. B. Kaidalov and Y. .A. Simonov, “Odderon and pomeron from the vacuum correlator method,” Phys. Lett. B **636**, 101 (2006) [hep-ph/0512151].
- [67] V. Mathieu, C. Semay and B. Silvestre-Brac, “Semirelativistic potential model for three-gluon glueballs,” Phys. Rev. D **77**, 094009 (2008) [hep-ph/0803.0815].
- [68] S. Godfrey and J. Napolitano, “Light meson spectroscopy,” Rev. Mod. Phys. **71**, 1411 (1999) [hep-ph/9811410].
- [69] M. Tanabashi *et al.* [Particle Data Group], “Review of Particle Physics,” Phys. Rev. D **98**, no. 3, 030001 (2018).
- [70] T. Gherghetta, J. I. Kapusta and T. M. Kelley, “Chiral symmetry breaking in the soft-wall AdS/QCD model,” Phys. Rev. D **79**, 076003 (2009) [arXiv:0902.1998 [hep-ph]].
- [71] T. M. Kelley, “The Dynamics and Thermodynamics of Soft-Wall AdS/QCD,” arXiv:1108.0653 [hep-ph].
- [72] A. V. Anisovich, V. V. Anisovich and A. V. Sarantsev, “Systematics of  $q$  anti- $q$  states in the  $(n, M^{**2})$  and  $(J, M^{**2})$  planes,” Phys. Rev. D **62**, 051502 (2000) [hep-ph/0003113].
- [73] D. Ebert, R. N. Faustov and V. O. Galkin, “Mass spectra and Regge trajectories of light mesons in the relativistic quark model,” Phys. Rev. D **79**, 114029 (2009) [arXiv:0903.5183 [hep-ph]].
- [74] J. K. Chen, “Concavity of the meson Regge trajectories,” Phys. Lett. B **786**, 477 (2018) [arXiv:1807.11003 [hep-ph]].
- [75] F. Iachello, N. C. Mukhopadhyay and L. Zhang, “Spectrum generating algebra for string like mesons. 1. Mass formula for  $q$  anti- $q$  mesons,” Phys. Rev. D **44**, 898 (1991).
- [76] E. Klempt and J. M. Richard, “Baryon spectroscopy,” Rev. Mod. Phys. **82**, 1095 (2010) [arXiv:0901.2055 [hep-ph]].
- [77] E. Klempt, “Baryon resonances and strong QCD,” nucl-ex/0203002.
- [78] M. Henningson and K. Sfetsos, “Spinors and the AdS / CFT correspondence,” Phys. Lett. B **431**, 63 (1998) [hep-th/9803251].
- [79] W. Mueck and K. S. Viswanathan, “Conformal field theory correlators from classical field theory on anti-de Sitter space. 2. Vector and spinor fields,” Phys. Rev. D **58**, 106006 (1998) [hep-th/9805145].
- [80] Z. Abidin and C. E. Carlson, “Nucleon electromagnetic and gravitational form factors from holography,” Phys. Rev. D **79**, 115003 (2009) [arXiv:0903.4818 [hep-ph]].

- [81] J. H. Gao and Z. G. Mou, “Polarized Deep Inelastic Scattering Off the Neutron From Gauge/String Duality,” *Phys. Rev. D* **81**, 096006 (2010) [arXiv:1003.3066 [hep-ph]].
- [82] E. Klempt, “A Mass formula for baryon resonances,” *Phys. Rev. C* **66**, 058201 (2002) [hep-ex/0206012].
- [83] D. V. Bugg, “Four sorts of meson,” *Phys. Rept.* **397**, 257 (2004) [hep-ex/0412045].